Citation for published version:
Rhead, A, Koisin, V & Butler, R 2014, 'Investigation of failure modes in impact damaged steered fibre laminates'.

Publication date:
2014

Document Version
Early version, also known as pre-print

Link to publication

University of Bath

Alternative formats
If you require this document in an alternative format, please contact:
openaccess@bath.ac.uk

General rights
Copyright and moral rights for the publications made accessible in the public portal are retained by the authors and/or other copyright owners and it is a condition of accessing publications that users recognise and abide by the legal requirements associated with these rights.

Take down policy
If you believe that this document breaches copyright please contact us providing details, and we will remove access to the work immediately and investigate your claim.

Download date: 05. May. 2023

INVESTIGATION OF FAILURE MODES IN IMPACT DAMAGED STEERED FIBRE LAMINATES

A.T. Rhead, V. Koissin and R. Butler

Department of Mechanical Engineering, University of Bath, UK

Abstract: *Continuous Tow Shearing (CTS) is a novel form of fibre steering technology which can produce optimised laminated composite structures with improved buckling capacity and lower mass. The distribution of fibre orientation and mass across the width of these laminates that results from optimisation produces regions of high stress near supports. These regions, which are vital to the integrity of the CTS laminate, are at risk of reduction in compressive strength as a consequence of Barely Visible Impact Damage (BVID). In this paper straight fibre coupons, representing the high stiffness regions of the CTS laminate, are subject to compression testing to shed light on the intra-ply failure seen in the compression after impact testing of CTS laminates. A Tsai-Wu first ply failure analysis predicts experimental failure stress to within 14% for an undamaged coupon. This increases to 41% for damaged coupons where damage has seeded intra-ply cracking.*

Keywords: layered composite, tow steering, delamination, compression after impact, damage tolerance.

Nomenclature

E_{11} = Longitudinal elastic modulus
E_{22} = Transverse elastic modulus
G_{12} = Shear modulus
S_{1C} = Ultimate longitudinal stress in compression
S_{1T} = Ultimate longitudinal stress in tension
S_{12} = Ultimate shear stress
S_{22} = Ultimate transverse stress in tension and compression
t_0 = Unsheared ply thickness
t_θ = Sheared ply thickness for θ fibre path
t_ϕ = Sheared ply thickness for ϕ fibre path
ε^c = Applied axial strain at sublaminate buckling
ε_{ult} = Applied axial strain at laminate failure
$\varepsilon_{Tsai\text{-}Wu}$ = Strain at first ply failure predicted by a Tsai-Wu analysis
$\sigma_{Tsai\text{-}Wu}$ = Stress at first ply failure predicted by a Tsai-Wu analysis
σ_{ult} = Applied axial stress at laminate failure
ψ = Steered fibre path ply angle
θ = Straight fibre ply angle
ϕ = Steered fibre path ply angle
ν_{12} = Major Poisson's ratio

1. Introduction

Optimal load redistribution through steering of fibres can improve the buckling performance and reduce the weight of laminated composite panels. Continuous Tow Shearing (CTS) – a novel fibre steering technique – allows defect-free manufacture at tight radii of curvature that are not achievable with other fibre steering techniques [1]. Owing to the shear deformation of fibre tows, CTS produces panels with complex variable thickness geometries. CTS panels with an unsheared material thickness of 0.135mm (at 90**°**)**,** when optimized for minimum mass (subject to a minimum buckling load constraint and single axis compressive loading) offer a theoretical weight saving of 34% in comparison with a straight fibre laminate with ply thickness 0.15mm and optimized stacking sequence $[45/\text{-}45/0_2/\text{-}45/45/0_2/90/0]_S$ (where optimization was for the same support conditions and buckling constraints). Optimised CTS panels typically have a sinusoidal transverse thickness variation [2], see Fig. 1. Thickness maximizes near supports and is approximately quadruple that of central regions made from unsheared material. These thicker zones correspond to low fibre angles

and act as natural stiffeners, making them both highly stressed and also critical to panel load carrying capacity.

However, aerospace composite laminates are not only subject to design requirements for buckling resistance; designs such as that in Fig. 1 are still vulnerable to impact damage and material failures both of which can cause significant reduction in compressive strength. The present study aims to provide understanding of the failure modes of a buckling resistant CTS panel both with and without impact damage such that design improvements can be made. A summary of the CTS panel and its failure modes can be found in subsection 1.1. Here, the investigation of CTS failure modes is based on compression and compression after impact (CAI) testing of straight-fibre laminates which are representative of the vulnerable high-stress regions so important for the buckling resistance and damage tolerance of CTS panels. Sublaminate buckling and intra-ply cracking driven failures are identified. A further test was conducted on a coupon that included a core region of ±45° plies who purpose is to delay or prevent the formation of intra-ply failures. In all cases a comparison is made with a Tsai-Wu first ply failure analysis.

1.1 CTS panel design and failure

Figure 1(a) shows the steered fibre path and prismatic cross-section (indicating thickness variation) for a minimum mass buckling resistant CTS panel with stacking sequence $[+\psi/-\psi/-\phi/+\phi]_S$; ψ and ϕ describe continuous steered fibres paths. Steering of CTS fiber tows results in a fiber angle dependent increase in tow thickness from t_0 (unsheared) to t_ψ (sheared) where,

$$t_\psi = \frac{t_0}{sin(\psi)} \tag{1}$$

Table 1 gives the fibre angles ψ and ϕ and associated lamina thicknesses t_ψ and t_ϕ based on the strip discretisation in Fig. 1 (a).

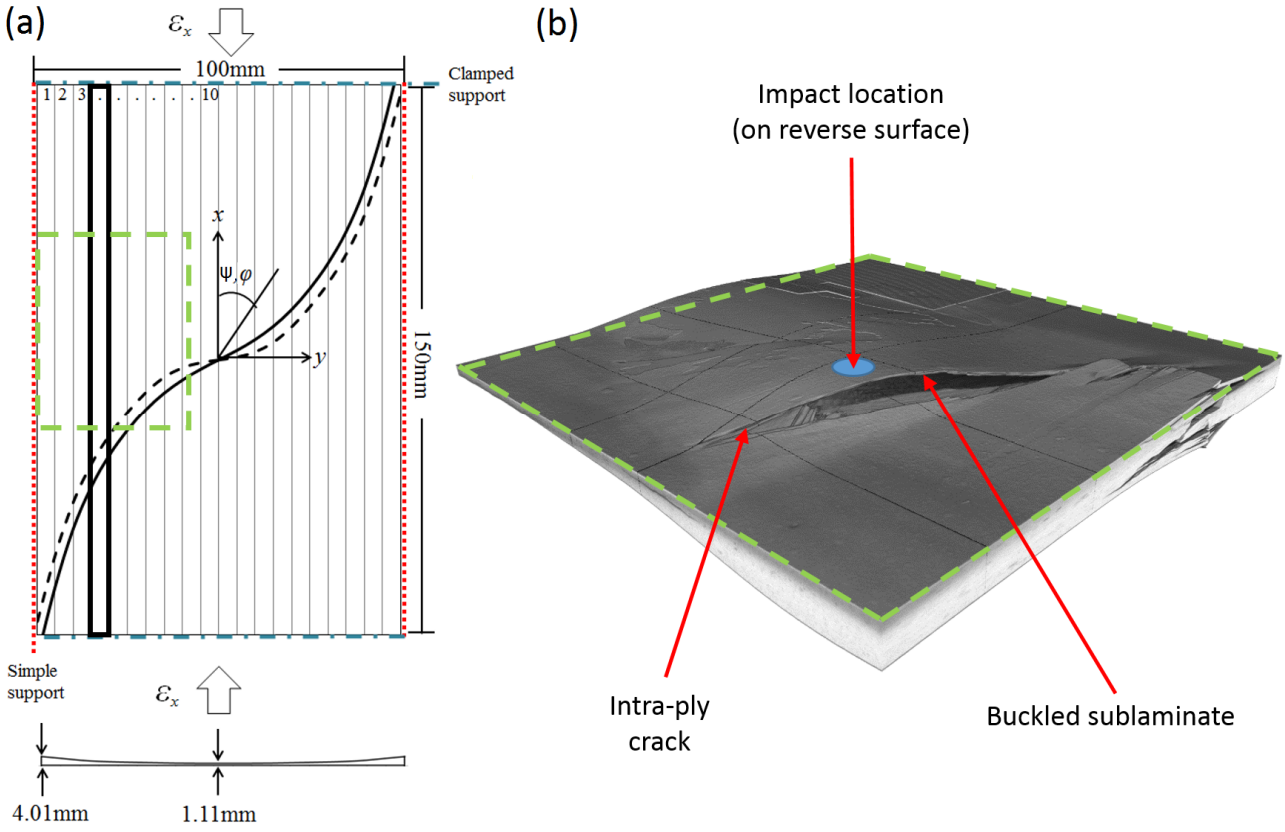

Fig.1. (a) Optimized CTS steered laminate showing (top) fibre angle distributions for ψ (solid curve) and ϕ (dashed curve) and (bottom) thickness distribution across the width. Sides are simply-supported and loading edges clamped. Load is applied as axial strain ε_x. Strip numbers in the top left corner correspond to Table 1. Dashed area is indicative of the extent of the CT image in (b). (b) X-ray CT image of CTS laminate following compression after impact testing.

In previous [3] and ongoing work CTS laminates were manufactured from Carbon Fibre Reinforced Plastic (CFRP) pre-preg with material properties E_{11} = 163 GPa, E_{22} = 6.8 GPa, G_{12} = 3.4 GPa, and ν_{12} = 0.28.

Compression testing was undertaken on three CTS panels; two of which were subject to 8J impacts. The pristine CTS laminate failed at 5460 μstrain and the impacted laminates at 5010 μstrain and 4510 μstrain where the difference is a consequence of the choice of impact surface with respect to the asymmetric laminate thickness profile. This represents a loss in strength of 9% and 18% respectively. Failure of the non-impacted coupon initiated in the region of the panel with the highest local Poisson's ratio (approximately ±32° fibres, see Table 1). In the impacted coupon tests post-test X-ray Computed Tomography (XRCT) images indicated failure initiated in the damaged region and a combination of sublaminate buckling and intra-ply cracking was identified as the failure mechanism, see Fig. 1(b). It has been shown [4,5] that in-plane matrix shearing is the key factor in the failure of undamaged laminates comprised of only ±θ° plies where 15° < θ < 50° which is the case for the present study.

Table 1: Buckling optimized CTS steered laminate fiber angle (ψ and ϕ) and lamina thickness (t_ψ and t_ϕ). Strip numbers relate to Fig.1.

Strip no.	1	2	3	4	5	6	7	8	9	10
ψ (deg.)	15.6	18.2	23.5	30.0	35.9	41.4	47.6	54.2	59.4	62.7
t_ψ (mm)	0.48	0.42	0.33	0.26	0.22	0.20	0.18	0.16	0.15	0.15
ϕ (deg.)	14.5	18.4	25.2	32.1	37.7	42.8	50.6	62.5	74.0	80.7
t_ϕ (mm)	0.52	0.41	0.31	0.24	0.21	0.19	0.17	0.15	0.14	0.13

2. Test methods

2.1. Test panel design

Owing to the combination of CTS ply thickness, high axial stiffness and high Poisson's ratio the region of the CTS panels with approximately ±32° local fibre angle was identified as being the most vulnerable to damage and in particular sublaminate buckling delamination driven propagation [6,7] (Strip 4 in Fig. 1 and Table 1).

Three coupons were manufactured from 0.185mm thick pre-preg Carbon Fibre Reinforced Plastic (CFRP) layers with material properties E_{11} = 146GPa, E_{22} = 12GPa, G_{12} = 5.2GPa, and ν_{12} = 0.15. Coupon stacking sequences are given in Table 2. Note that only core plies appear as single thickness plies in order to mimic the addition of unsheared non-CTS UD plies to a CTS laminate. All other layers appear in pairs mimicking the thickness increase caused by shearing tows from 90° to 32°, see [1] and Eq.(1). Coupons are referred to as $[\pm32]_P$, $[\pm32]_D$, and $[\pm45]_D$, where number refers to core ply angle, subscript p refers to pristine and subscript I to impacted, see Table 2. Two coupons with only ±32° plies were manufactured in order to compare the CAI strength of an impacted coupon with that of a pristine coupon. The third coupon was designed to inhibit intra-ply failure whilst introducing limited laminate coupling. Thickness was maintained across all coupons to ensure parity and hence, in a departure from the original CTS design, single thickness ±32° plies were added to the centre of the $[\pm32]_P$ and $[\pm32]_D$ laminates.

Table 2: Coupon ID's, stacking sequences, experimental results for sublaminate buckling (ε^c), and failure (ε_{ult}, σ_{ult}) and 1st ply failure analysis ($\varepsilon_{Tsai\text{-}Wu}$, $\sigma_{Tsai\text{-}Wu}$).

ID	Stacking sequence	ε^c (μstrain)	ε_{ult} (μstrain)	$\varepsilon_{Tsai\text{-}Wu}$ (μstrain)	σ_{ult} (MPa)	$\sigma_{Tsai\text{-}Wu}$ (MPa)
$[\pm32]_P$	$[32_2/-32_4/32_2/-32/32/32/-32/-32_2/32_4/-32_2]$	N/A	4700	6000	245.9	280
$[\pm32]_D$	$[32_2/-32_4/32_2/-32/32/32/-32/-32_2/32_4/-32_2]$	≈1500	3700	6000	198.1	280
$[\pm45]_I$	$[32_2/-32_4/32_2/-45/45/45/-45/-32_2/32_4/-32_2]$	≈1500	3900	6500	196.2	280

2.2. Impact

Coupons $[\pm 32]_D$ and $[\pm 45]_D$ were impacted with the third coupon $[\pm 32]_P$ retained as a pristine reference coupon. During impact coupons were clamped over a 75×125mm ASTM D7136 [8] impact window. A 15J low-velocity impact was delivered using an Instron Dynatup 9250 HV instrumented impact test machine, employing a 6.2 kg mass and a 16mm hemispherical tup. Pneumatic brakes prevented secondary impacts. Following impact, damage morphology was assessed using an Ultrasonic Sciences Ltd. C-scan system (with a 35 MHz probe) and a Nikon XT225H X-Ray Computed Tomography (XRCT) system.

2.3. Compression after impact

During the axial compression tests, laminates were fitted into a compression rig. The rig consists of two end fixtures producing fully clamped conditions and a circular anti-buckling guide of internal diameter 85mm, see Fig. 2.

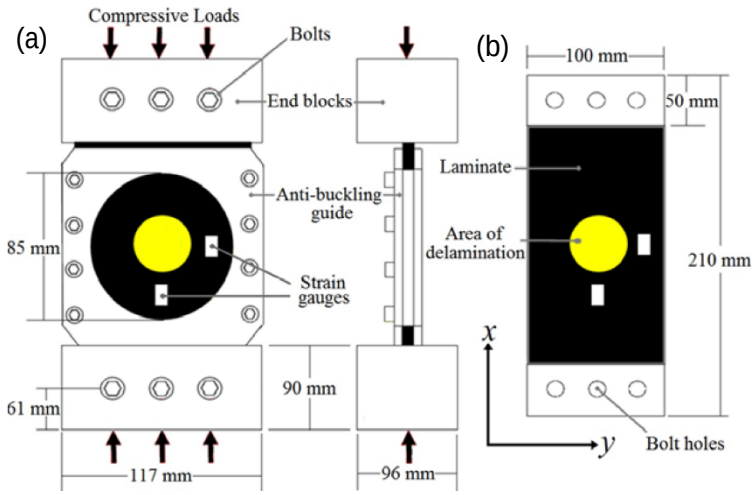

Fig. 2: Compression fixture with anti-buckling guide (a) and dimensions of coupon (b). Strain gauges are shown as white rectangles and are orientated vertically.

The anti-buckling guide restrains full laminate buckling, thereby resisting interaction of laminate and sublaminate buckling modes, but has a wide enough window to ensure delamination growth can occur unhindered. To ensure coupons were correctly aligned and placed under pure axial compression, strains were recorded throughout the tests by two pairs of vertically aligned back-to-back strain gauges, see Fig. 2. During the experiments, axial compression was applied in the x-direction under displacement control at 0.1mm/min until failure events were detected on strain gauge outputs. Buckling modes and failure sequences were monitored using a Digital Image Correlation (DIC) system which employs two pairs of stereo cameras to measure 3D surface displacement.

3. Experimental results

3.1. Impact

On the impacted face, dent depth was difficult to determine accurately but was certainly shallower than the industrial threshold depth (0.3mm) for BVID. However, visual and XRCT inspection identified surface cracks (of approximately 20-30 mm in length) along the fibre direction on the non-impacted face of the $[\pm 32]_D$ and $[\pm 45]_D$ coupons. This suggests that damage may actually be classified as clearly visible despite the small dent depth. A small residual out-plane deformation of the non-impact face was also observed. Figure 3 shows impact data for load and energy versus time after impact for the $[\pm 32]_D$ and $[\pm 45]_D$ coupons.

Figures 4(a) and 5(a) shows XRCT images of damage in the $[\pm 32]_D$ and $[\pm 45]_D$ coupons respectively. The largest delaminations are attributed to the 2nd (+32°/-32°, 0.37mm from the surface) and 6th (-

32°/+32°, 1.11mm from the surface) interfaces which are co-incident with the boundaries of ply blocks, see Table 2 and Figs. 4(a) and 5(a). The 2nd interface delaminations are connected with intra-ply surface cracks.

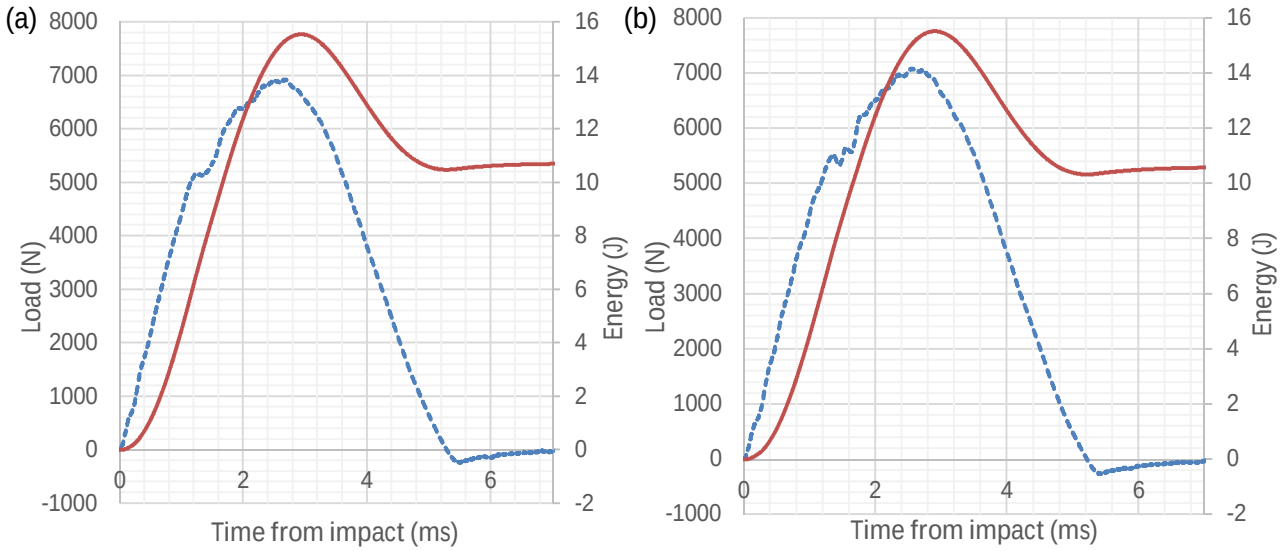

Fig. 3 Impact data for (a) $[\pm 32]_D$, and (b) $[\pm 45]_D$ coupons. Dashed lines are load time traces and solid are energy time traces following impact.

3.2. Compression after impact

Experimental results for sublaminate buckling and ultimate failure are listed in Table 1. Failure strains reported in Table 2 are an average of all four strain gauges (see Fig. 6) correlated with sublaminate buckling and failure events observed using the DIC system, see Fig. 4(b) and (c) and 5 (b) and (c).

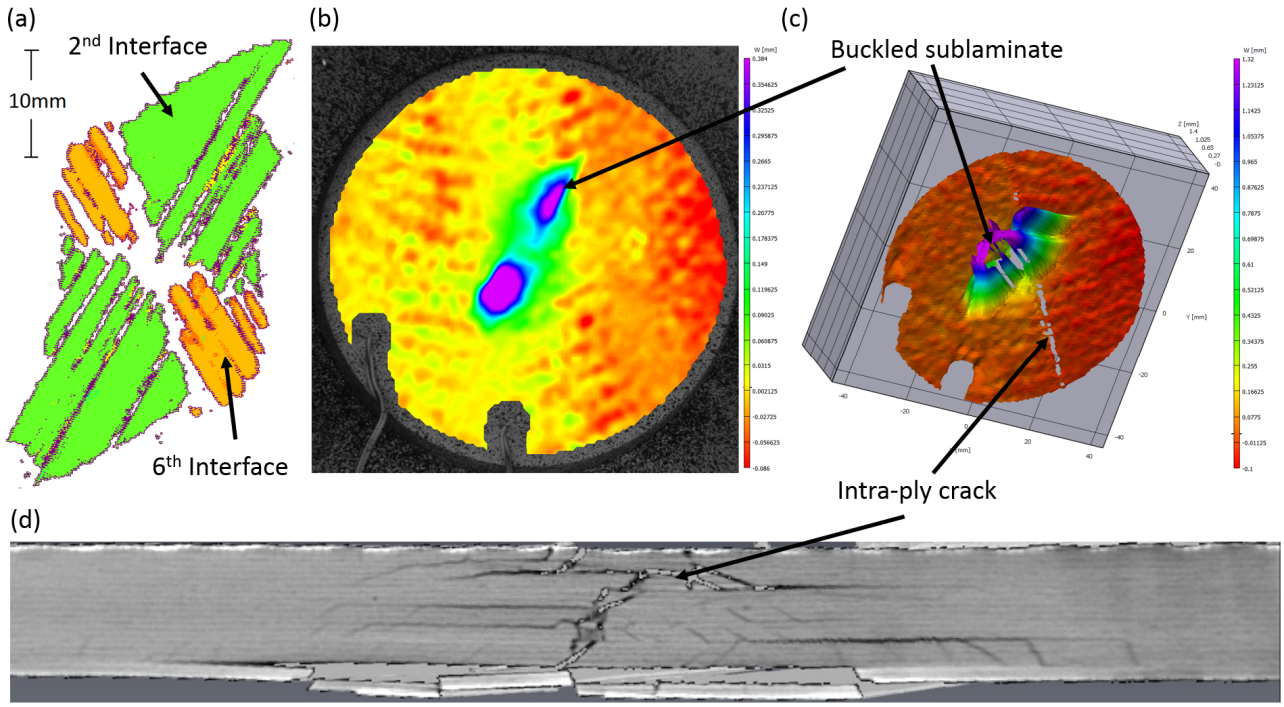

Fig. 4 Failure sequence of the $[\pm 32]_D$ coupon: (a) C-scan image from the non-impact surface of damage prior to compression. (b) 2D DIC image of fully formed 2-ply sublaminate buckles above the 1st interface (62kN). (c) 3D DIC image taken immediately after failure (note the large intra-ply crack on the laminate surface). (d) X-ray CT image of impact damage following failure.

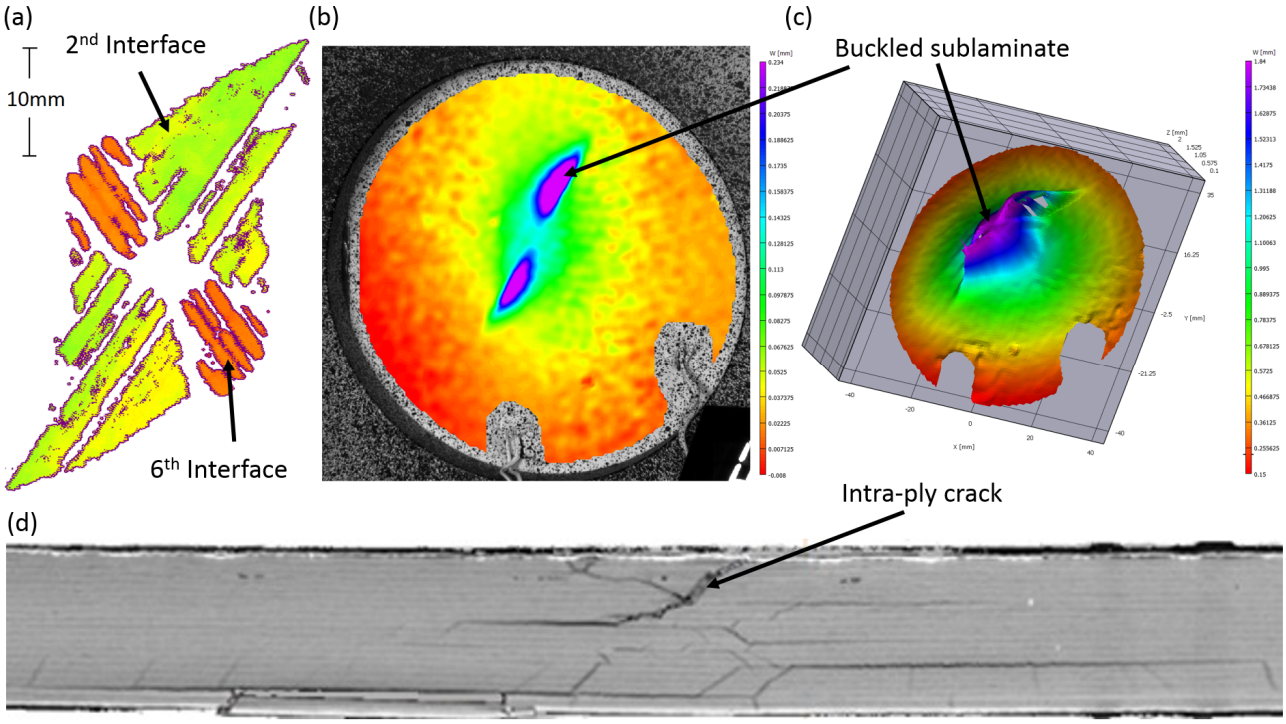

Fig. 5 Failure sequence of the $[\pm45]_D$ coupon: (a) C-scan image from the non-impact surface of damage prior to compression. (b) 2D DIC image of fully formed 2-ply sublaminate buckles above the 1st interface (42kN). (c) 3D DIC image taken immediately after failure (note the large intra-ply crack on the laminate surface. (d) X-ray CT image of impact damage following failure.

The $[\pm32]_P$ coupon failed following the occurrence of a 32° intra-ply crack which traversed the whole laminate thickness. Crack initiation was noted at 84kN (4200 μstrain), noted as a kink in the strain gauge output in Fig. 6(a) and was likely the initial failure of the matrix in the 32° plies. This reduced the support of the -32° fibres eventually leading to fibre breakage and coupon failure.

In the $[\pm32]_D$ test sublaminate buckling (see Fig. 4(b)) occurred above both lobes of the 2nd ply interface delamination and at about 35kN (1500 μstrain). Failure occurred suddenly – over a single DIC frame – at 73.3kN (3700 μstrain) as a result of a shear-driven intra-ply crack forming at 32°, see Figs. 4(c) and (d). This crack passed through the centre of the damaged region and extended to the coupon edges.

In the $[\pm45]_D$ test sublaminate buckling again occurred above both lobes of the 2nd ply-interface delamination at approximately 30kN (1500 μstrain) (see Fig. 5(b)). Global laminate buckling developed during the latter stages of the test with deflection toward the non-impact surface. The amplitude of this movement was much larger than that observed for the $[\pm32]_D$ impacted coupon, and created a closed-form sublaminate buckling modeshape. The test was stopped at 72kN (4000 μstrain) following significant cracking and strain gauge divergence. Fig. 5(d) shows a post CAI-test XRCT image which indicates that an intra-ply crack has been initiated and was probably interacting with the global buckling of the laminate.

XRCT images taken after the compression tests reveal that for both impacted coupons the failure was likely a result of a shear-driven intra-ply crack(s) forming in the core of the damaged region. This is illustrated in Figs. 4(d) and 5(d) which show large intra-ply cracks traversing all ±32° layers. These cracks are arrested by the ±45° layers, as seen at the mid-plane of the $[\pm45]_D$ coupon, see Fig. 5(d). A number of such cracks initiated during the loading but the final failure owing to fibre breakage localised to a single crack. DIC analysis, post-CAI XRCT and C-scan imaging indicate that no delamination propagation occurred before failure.

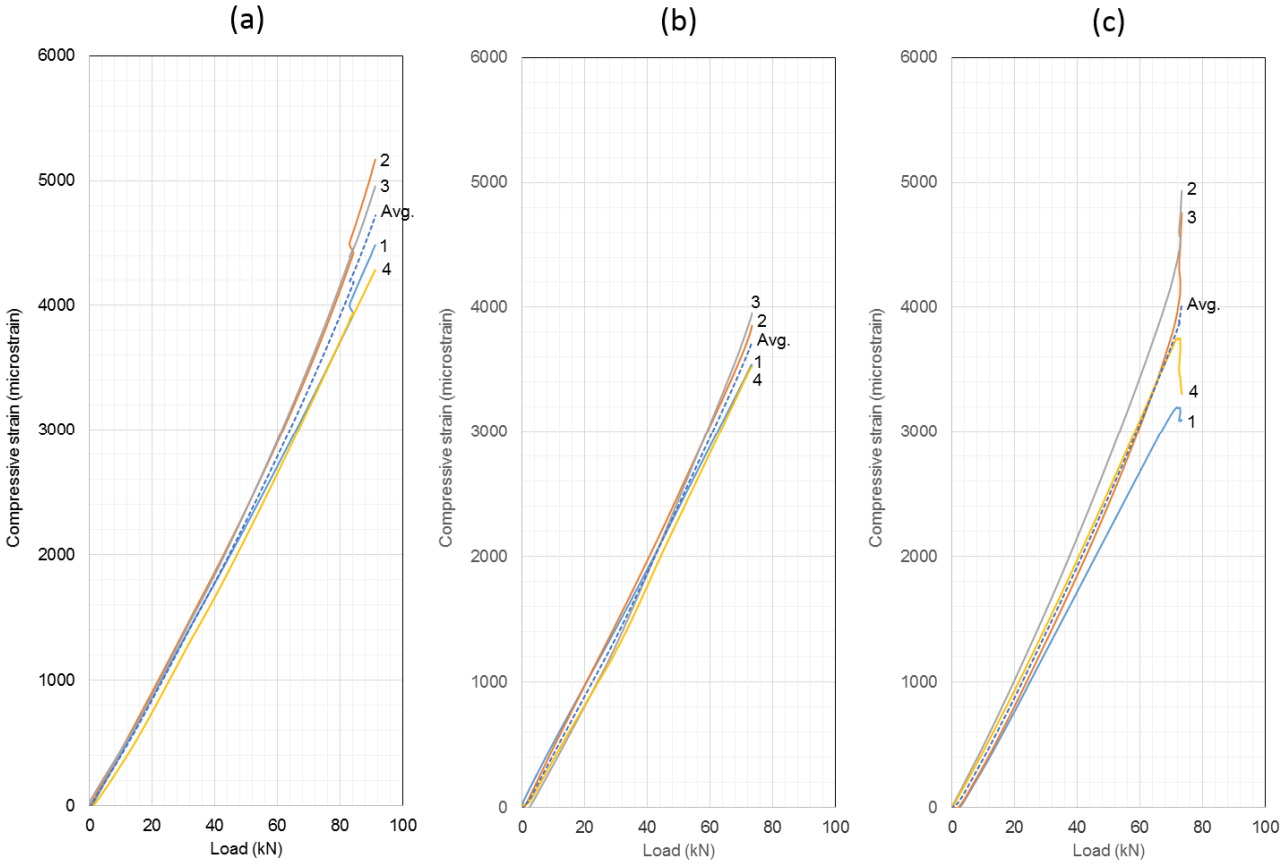

Fig.6: Load vs. strain gauge readings for the (a) $[\pm 32]_P$, (b) $[\pm 32]_I$ and (c) $[\pm 45]_I$ coupons respectively.

4. In-plane failure analysis

A Tsai-Wu first-ply failure criterion was employed (using LAP software [9]) to ascertain whether coupon failure was linked to intra-ply cracking, see Fig. 7. The following strength properties were used for UD layers: S_{1T} = 3050 MPa (ultimate longitudinal stress in tension), S_{1C} = 1500 MPa (ultimate longitudinal stress in compression), S_{12} = 94 MPa (ultimate stress in shear) , and S_{22} = 70 MPa (ultimate transverse stress) is assumed for both tension and compression. A comparison is made between $[\theta_2/-\theta_4/\theta_2/-\theta/\theta/\theta/-\theta/-\theta_2/\theta_4/-\theta_2]$ (ID = $[\pm\theta]$) and $[\theta_2/-\theta_4/\theta_2/-45/45/45/-45/-\theta_2/\theta_4/-\theta_2]$ (ID = [±θ/±45 core]) laminates where θ is allowed to vary between 0° and 90°. Note that Tsai-Wu failure analysis assume no transverse constraint/load is applied to the laminate. However, in all compression tests (CTS and straight fibre) transverse expansion was restrained by clamped end conditions.

Figure 7(a) shows that intra-ply crack bridging layers offer no increase in stress for $\theta \approx 30°$ although they are beneficial for $\theta > 45°$. Figure 7(b) reveals that for $15° < \theta < 40°$ the [±θ/±45 core] design offers improve strain to failure in comparison to the $[\pm\theta]$ design, with the largest benefit occurring for $20° < \theta < 25°$. For the particular case of $\theta = 32°$, the intra-ply crack bridging layers increase the failure strain by 12%. Comparison with experimental results shows the intra-ply crack bridging layers had a similar effect.

5. Discussion

As shown in Fig. 3, the response to impact of the $[\pm 32]_D$ and $[\pm 45]_D$ coupons is almost identical differing only slightly in the load vs. time impact trace at about 1.5ms. This is likely a consequence of the ±45 layers in $[\pm 45]_D$ coupon deflecting the formation of intra-ply cracking and delamination. This similarity of damage is also seen in C-scan images of test coupons in Figs. 4(a) and 5(a) which show damage of similar size and shape for both coupons.

The $[\pm 32]_D$ coupon failed at 80% (79%) of the $[\pm 32]_P$ coupon failure stress (strain). Similarly, the $[\pm 45]_D$ coupon failed at 80% (83%) of the $[\pm 32]_P$ coupon failure stress (strain).

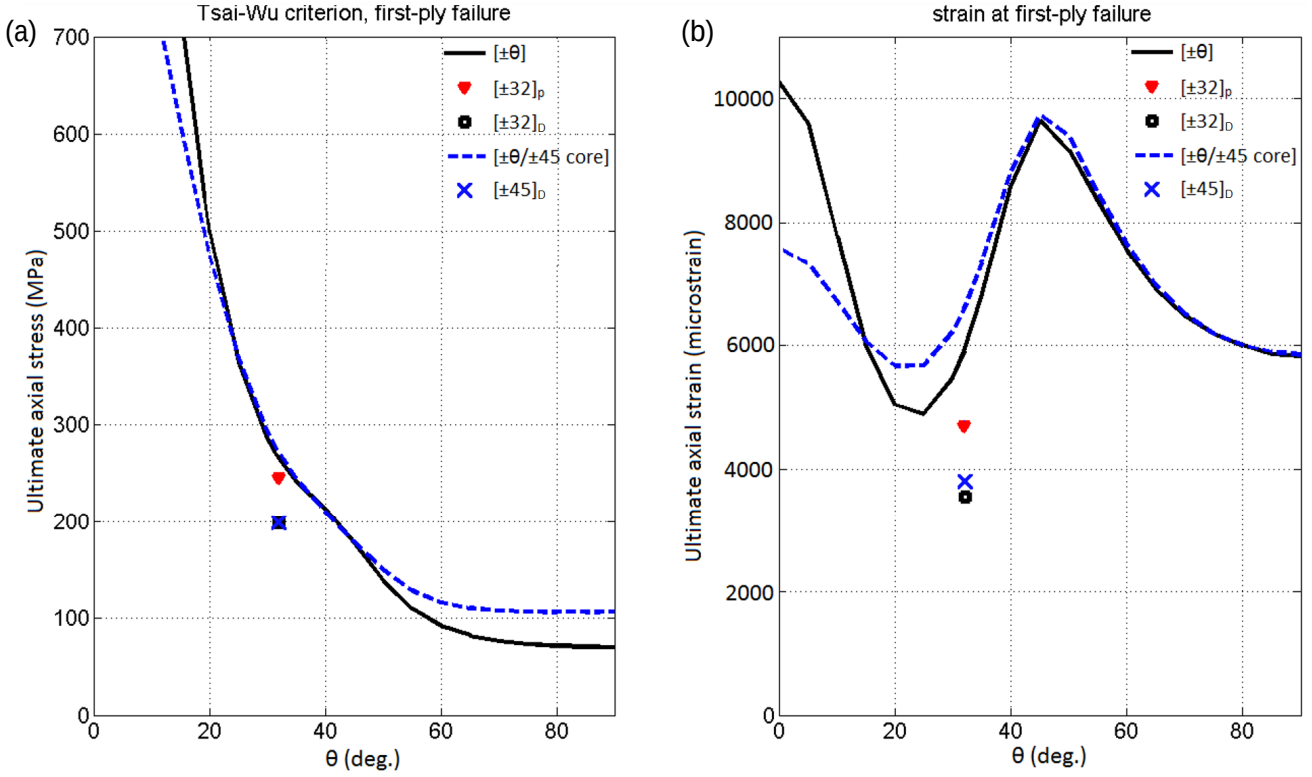

Fig.7: Comparison of the first-ply failure (a) stress and (b) strain for the [±θ] and [±θ/±45 core] laminate constitutions, under uniaxial compression.

The failure mode in all coupons was principally intra-ply cracking in the resin matrix localising to a single crack leaving fibres across it unsupported and subject to a shearing/kink-band-like failure.In the case of the $[\pm 32]_P$ and $[\pm 32]_D$ coupons the final intra-ply crack travelled through the entire thickness of the laminate, see Fig. 4(d). In the case of the $[\pm 45]_D$ coupon the centrally located plies arrested the intra-play crack that had spread from inward from both surfaces of the laminate, see Fig. 5(d). However, the formation of the crack through the majority of the laminate significantly lowered the coupon's out-of-plane stiffness and seemed to enable a global buckling response as is seen in Fig. 5(c) and also via the significant divergence of strain gauge readings in Fig. 6(c). It is possible that laminate coupling caused by the addition of ±45° layers may have contributed to the out-of-plane response of the $[\pm 45]_D$ coupon. Addition of ±45° layers on the surface of the laminate may delay both intra-ply cracking and laminate buckling.

The failure stress predicted by a Tsai-Wu first ply failure analysis in Fig. 7(a) was within 14% of the experimental result for the $[\pm 32]_P$ coupon. The failure strain of the $[\pm 32]_P$ coupon was over predicted by 28%, see Fig. 7(b). This is a consequence of the disparity between assumed boundary conditions in the Tsai-Wu analysis and those found in the experiment. Uncertainty in material properties and failure stresses used in the Tsai-Wu analysis are also likely to have contributed to the discrepancy.

Unsurprisingly, damaged coupon stresses to failure were over predicted by approximately 42% for both the $[\pm 32]_D$ and $[\pm 45]_D$ coupons. A similar knock-down is seen in strain to failure, see Fig. 7(b). This is a consequence of impact damage causing partial intra-ply cracking which will have seeded the formation of the final failure crack. This is illustrated by the position of the final failure cracks through the centre of the damaged region in both coupons, see Figs. 4(d) and 5(d). However, relative strength was correctly predicted by Tsai-Wu in that equality of experimental failure stress for the $[\pm 32]_D$ and $[\pm 45]_D$ coupons was correctly predicted, see Fig. 7(a). Similarly the marginally higher strain to failure of the $[\pm 45]_D$ coupon in comparison to the $[\pm 32]_P$ coupon was also predicted, see Fig. 7(b).

Reductions in pristine strength owing to impact damage were similar for both CTS (9-18%) and straight fibre coupons (17-21%). This supports the case for intra-ply cracking being the likely cause of failure for the CTS laminates.

6. Conclusions

Three straight fibre coupons, ($[\pm32]_P$, $[\pm32]_D$ and $[\pm45]_D$) representative of the local stacking sequence in a highly stressed region of a Continuous Tow Shearing (CTS) steered fibre panel, were compression tested to failure. Two coupons ($[\pm32]_D$ and $[\pm45]_D$) were impacted before compression testing, of which the $[\pm45]_D$ coupon contained additional fibres in order to restrict intra-ply crack growth. Two failure mechanisms were identified in the compression after impact test; sublaminate buckling and intra-ply cracking. Most significant was intra-ply cracking as it led to final failure.

Reductions in pristine strength owing to impact damage were similar for both CTS (9-18%) and straight fibre coupons (17-21%). Indicating intra-ply cracking is the likely cause of failure of previously tested CTS laminates.

Impact damage caused a reduction in compressive strength as it seeded the laminate with intra-ply cracks hastening failure via contiguous through-thickness intra-ply cracking. The additional ±45° fibres in the $[\pm45]_D$ coupon successfully prevented an intra-ply from traversing the entire thickness of the laminate. This improvied strain to failure by 4% but also reducing stress to failure by 1.5%. Hence the addition of ±45° fibres to the core a CTS panel would be insufficient to improve panel strength.

The failure stress predicted by a Tsai-Wu first ply failure analysis was within 14% of the experimental result for the undamaged $[\pm32]_P$ coupon. Damaged coupon stresses to failure were over predicted by the Tsai-Wu failure criteria by approximately 42% as it does not account for the effect of damage on strength.

7. Future work

It is anticipated that the CAI strength can be improved by further modifying the stacking sequence of the internal layers to suppress in-plane shear failure [7]. The effect of design variables such as the thickness and orientation of additional surface plies on damage tolerant strength should also be addressed.

Acknowledgements

The authors gratefully acknowledge the assistance of Dr Byung Chul Kim (University of Bristol) with impact testing. The second author was supported through Engineering and Physical Sciences Research Council grant EP/H025898/1. The third author is supported by a Royal Academy of Engineering/GKN Aerospace Chair in Composites Analysis.

References:

[1]: B.C. Kim, K. Potter, and P.M. Weaver. Continuous tow shearing for manufacturing variable angle tow composites. Composites: Part A 43 (2012) 1347-1356.

[2]: W. Liu, R. Butler, and A.T. Rhead. Optimized fiber steering and layer stacking for elastically tailored, damage tolerant laminates. In: Proc. of ICCM-19, July 28 - August 2, Montreal, Canada, pp.4436-4443.

[3]: A.T. Rhead, R. Butler, W. Liu, B.C. Kim, and S.R.Hallett. Compression after impact strength of a buckling resistant, tow steered panel. In: Proc. of ICCM-19, July 28 - August 2, Montreal, Canada, pp.4960-4969.

[4]: M.J. Shuart and J.G. Williams. Compression behavior of ±45°-dominated laminates with a circular hole or impact damage. AIAA Journal 1 (1986) 115-122.

[5]: M.J. Shuart. Failure of compression-loaded multidirectional composite laminates. AIAA Journal 9 (1989) 1274-1279.

[6]: R. Butler, A.T. Rhead, W. Liu, and N. Kontis. Compressive strength of delaminated aerospace composites. Phil. Trans. R. Soc. A. 370 (2012) 1759-1779.

[7]: A.T. Rhead, R. Butler, W. Liu, and N. Baker. The influence of surface ply fibre angle on the compressive strength of composite laminates containing delamination. The Aeronautical Journal. 1186 (2012) 1315-1330.

[8]: ASTM international. Standard Test Method for Measuring the Damage Resistance of a Fiber-Reinforced Polymer Matrix Composite to a Drop-Weight Impact Event, ASTM D7136 / D7136M - 12, 2012.

[9]: Analglyph Limited, London, UK. Laminate Analysis Program, 2014. http://www.anaglyph.co.uk/LAP.htm. Accessed: 18/09/2014.

[10]: HexPly® M21 Product datasheet. http://www.hexcel.com/Resources/DataSheets/Prepreg-Data-Sheets/M21_global.pdf. Accessed: 18/09/2014.